Asymmetric acoustic transmission through near-zero-index and gradient-index metasurfaces

Chen Shen,[1,a)] Yangbo Xie,[2,a)] Junfei Li,[2] Steven A. Cummer,[2,b)] and Yun Jing[1,b)]
[1]*Department of Mechanical and Aerospace Engineering, North Carolina State University, Raleigh, North Carolina 27695, USA*
[2]*Department of Electrical and Computer Engineering, Duke University, Durham, North Carolina 27708, USA*

(Received 30 March 2016; accepted 24 May 2016; published online 2 June 2016)

We present a design of acoustic metasurfaces yielding asymmetric transmission within a certain frequency band. The design consists of a layer of gradient-index metasurface and a layer of low refractive index metasurface. Incident waves are controlled in a wave vector dependent manner to create strong asymmetric transmission. Numerical simulations show that the approach provides high transmission contrast between the two incident directions within the designed frequency band. This is further verified by experiments. Compared to previous designs, the proposed approach yields a compact and planar device. Our design may find applications in various scenarios such as noise control and therapeutic ultrasound. *Published by AIP Publishing.*
[http://dx.doi.org/10.1063/1.4953264]

Asymmetric transmission, in which an incident wave is blocked from one direction while allowed for transmission from another, adds the flexibility to control the direction of the wave energy flow. Significant research efforts have been made to studying one-way manipulation of waves for both electromagnetic (EM) waves[1,2] and acoustic waves.[3–15] In the acoustic regime, several design strategies have been proposed to realize asymmetric transmission, in both linear[5–9,11–13] and nonlinear systems.[3,4,10] While nonreciprocal systems generally offer high transmission contrast, reciprocal but asymmetric systems can be good alternatives, with generally reduced system complexities, to provide similar one-directional functionality. Besides, such asymmetric and reciprocal systems can be designed entirely with passive structures that do not change the frequency content of the sound as may occur in nonlinear systems.[16] These asymmetric systems, however, are commonly associated with bulky structures. Recently, the emergence of acoustic metasurfaces opens up more possibilities in manipulating acoustic waves by controlling the reflection/refraction behaviors.[17–21] An acoustic open tunnel with metasurfaces attached to the walls has been proposed to allow sound transmission only in one direction.[12] Although asymmetric transmission is realized based on the phase engineering through the tunnel walls, the scheme requires the presence of a tunnel and its cross-sectional dimension to be comparable to the working wavelength, which poses limitations to its application. One-way acoustic metasurfaces with flat geometry can be readily integrated with existing surfaces (e.g., a wall or a planar transducer), and are highly desirable in the acoustic community since such metasurfaces allow easy application to various real-world needs.

In this letter, we investigate dual-layer flat and thin metasurfaces and their application to asymmetric transmission. The working principle of the metasurfaces reveals that, for incident waves with different directions, tunneling/total reflection will occur for the proposed structure. The transmission coefficients will thus have an asymmetric behavior in different directions. Both numerical simulations and experiments are carried out to verify the proposed structure. The geometry of the structure is flat so that it can be easily integrated with other structures, enabling a wide range of applications. The realization of asymmetric transmission in such a linear device may offer possibilities in controlling acoustics waves in various applications, such as therapeutic ultrasound and architectural acoustics.

The proposed device is composed of two layers: a near-zero index metasurface (ZIM) and a gradient-index metasurface (GIM), both having subwavelength thickness at the operating frequency as illustrated in Fig. 1. Consider a plane wave impinging normally on the GIM (Fig. 1(a)), the transmitted wave will travel at an angle dictated by the generalized Snell's law[22]

$$(\sin\theta_t - \sin\theta_i)k_0 = \mathrm{d}\Phi/\mathrm{d}x, \tag{1}$$

where θ_t and θ_i are transmitted and incident angles, k_0 is the wave number, and $\mathrm{d}\Phi/\mathrm{d}x$ is the phase gradient along the surface. For normal incidence, the refracted angle θ_t will have a certain non-zero value as θ_i is equal to zero. When the acoustic waves reach the interface between ZIM and GIM, total

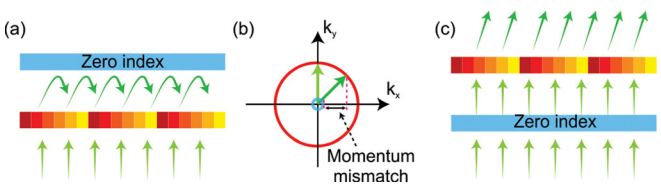

FIG. 1. Schematic of the working principle of the device. (a) Low transmission case where the incident wave faces the GIM. (b) k-space diagram showing that the rotation of momentum vector causes its mismatch in transverse components, leading to the low transmission. (c) High transmission case where the incident wave faces the ZIM.

[a)]C. Shen and Y. Xie contributed equally to this work.
[b)]Authors to whom correspondence should be addressed. Electronic addresses: cummer@ee.duke.edu and yjing2@ncsu.edu

Reuse of AIP Publishing content is subject to the terms at: https://publishing.aip.org/authors/rights-and-permissions. Download to IP: 152.14.115.167 On: Thu, 02 Jun 2016 18:24:35

reflection will occur if the incident angle is greater than the critical angle of the ZIM. Since the effective phase velocity of the ZIM is much greater than that of air, i.e., $v_{ZIM} \gg v_0$, the critical angle is close to zero as $\theta_c = \sin^{-1}(v_0/v_{ZIM})$. Consequently, the transmission coefficient in this direction is very low. This can be understood by the momentum mismatch at the interface when the incident angle is above the critical angle, as illustrated in Fig. 1(b). On the other hand, for acoustic waves propagating from the opposite direction, the incident wave reaches the ZIM at the normal direction and will pass through the ZIM with high transmission due to the tunneling effect,[23–25] as indicated by Fig. 1(c). The unit cells in the GIM are designed to yield a relatively high transmission coefficient. As a result, the overall transmission coefficient is expected to be high in this case. The transmitted wavefront will also be redirected because of the phase gradient along the GIM surface. It is noted that for this high transmission case, the transmitted wave will be redirected compared with the incident wave as illustrated by Fig. 1(c), dictated by the reciprocity in such a linear system.[16] In contrast to the previous asymmetric devices utilizing total internal reflection,[9,16] the metasurfaces proposed here combine the concept of the ZIM and GIM, making the profile planar and thinner.

To design the ZIM and GIM, labyrinthine metamaterials are used.[25] It should be pointed out that the general strategy for realizing asymmetric transmission in this paper is not restricted to the labyrinthine metamaterials, other candidates with the same required parameters can also be adopted, such as membrane-based structures.[26] For the ZIM, a type of labyrinthine structure is used which consists of subwavelength curled channels. The geometry of a single unit cell is the same as that in an earlier study[27] and is depicted in Fig. 2(a). The labyrinthine unit has a width $d_1 = 26$ mm, and the thickness of the channels and hard walls are 1.5 mm and 1 mm, respectively. The walls are 3-D printed with acrylonitrile butadiene styrene (ABS) plastic with density 1230 kg/m^3 and speed of sound 2230 m/s, and are assumed to be acoustically hard since their impedance is much greater than that of air. The effective refractive index for this structure is retrieved numerically using an inverse method,[28] and the results are plotted in Fig. 3. The background medium is air, with the density and speed of sound 1.2 kg/m^3 and 343 m/s, respectively. It can be seen that the refractive index of the proposed structure is close to zero at the operating frequency (around 3.1 kHz). The ZIM is thus acoustically transparent for incoming waves with normal incidence and opaque for oblique incident angles at working frequencies. To ensure sufficient energy contrast, two layers of the ZIM are used for the proposed device. The spiral structures of the GIM are adopted from a previous study, which showed extraordinary

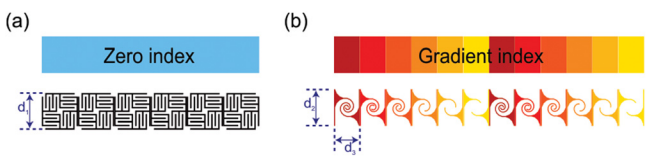

FIG. 2. The geometry of the metasurfaces (a) ZIM. (b) GIM. Top panels show the relative phase change across the unit cells.

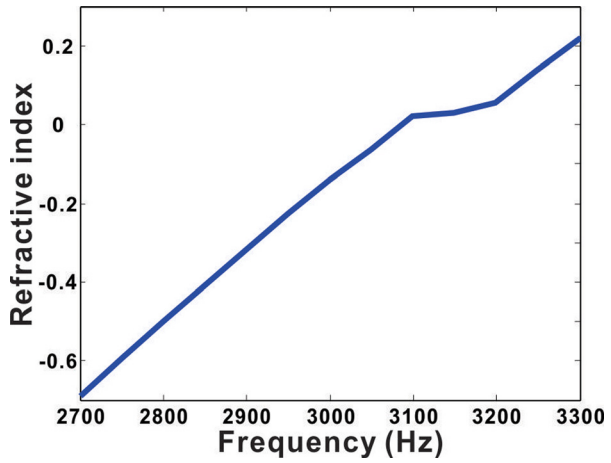

FIG. 3. Retrieved refractive index of a ZIM unit cell. The index is close to zero around 3.1 kHz.

capabilities in manipulating transmitted wavefronts.[20] Fig. 2(b) shows the geometry of the GIM, which consists of six types of individual unit cells. For the unit cells designed here, the transmitted phase difference across adjacent unit cells is about $\pi/6$, and two layers of the unit cells can cover a complete 2π of phase change for one period (6 unit cells). The relative phase difference can be preserved over a broad bandwidth and can be found in Ref. 20. The proposed GIM is thus expected to have a wavefront-bending effect around 3.0 kHz. The unit cells have identical thickness $d_2 = 34$ mm and width $d_3 = 26$ mm, thus making the GIM planar and easy for integration with existing surfaces. At 3.1 kHz, the phase gradient along the surface of the GIM is $d\Phi/dx = 40.3$ rad/m, and the corresponding transmitted angle can be calculated as 45.2° (assuming the incident angle is 0°) according to Eq. (1).

To verify the performance of the proposed structures, simulations using finite element package COMSOL Multiphysics and measurements of the prototype are carried out. Perfect matched layers (PML) are used in the simulations to minimize reflections from the boundaries. The experimental setup is shown in Fig. 4, where a loudspeaker array sends Gaussian beams with a center frequency at 3.0 kHz towards the metasurfaces. The metasurfaces are secured in a two-dimensional (2D) waveguide, with absorbing foams placed on

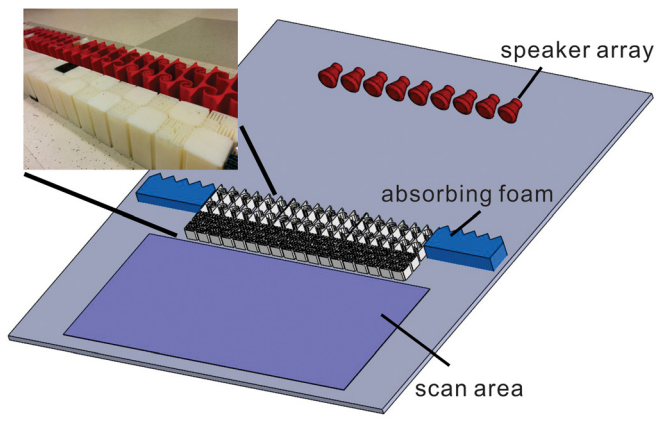

FIG. 4. Simulation and experimental setup. The inset shows the photo of the fabricated sample.

Reuse of AIP Publishing content is subject to the terms at: https://publishing.aip.org/authors/rights-and-permissions. Download to IP: 152.14.115.167 On: Thu, 02 Jun 2016 18:24:35

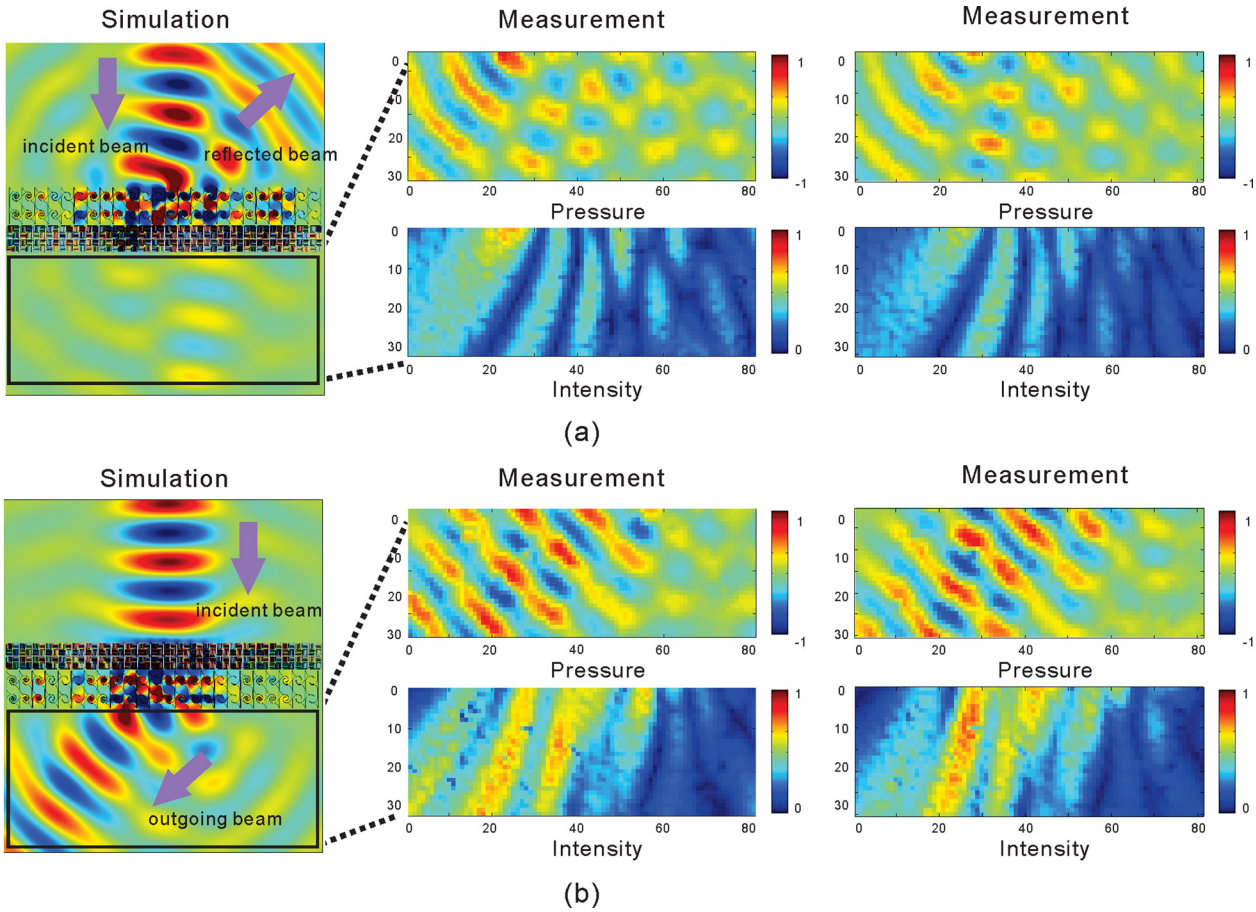

FIG. 5. Simulated and measured acoustic fields for incident waves in different directions. Left panels show the simulated acoustic pressure fields at 3.1 kHz. Middle and right panels show the measured acoustic pressure and intensity fields in the scan area at 3.1 kHz and 3.28 kHz, respectively. Axis unit: cm. (a) Incident beam is facing the GIM, corresponding to the low transmission case. (b) Incident beam is facing the ZIM, corresponding to the high transmission case.

both sides to prevent acoustic waves bypassing them. The field behind the metasurfaces is scanned with a moving microphone with a 2 cm step size. The signals are averaged with five measurements. The acoustic pressure field at different frequencies is then obtained by the inverse Fourier transform. Two sets of simulations and measurements are performed by swapping the direction of the incoming wave.

The fabricated device is shown in the inset of Fig. 4, where the red structure on the top is GIM and the white structure on the bottom is ZIM. The overall size of the device is 63 cm × 12 cm, and the thickness is about one wavelength at the operating frequency. The acoustic fields in the scan area for simulation and measurement are illustrated in Fig. 5 at 3.1 kHz. The right panels also show the measured acoustic

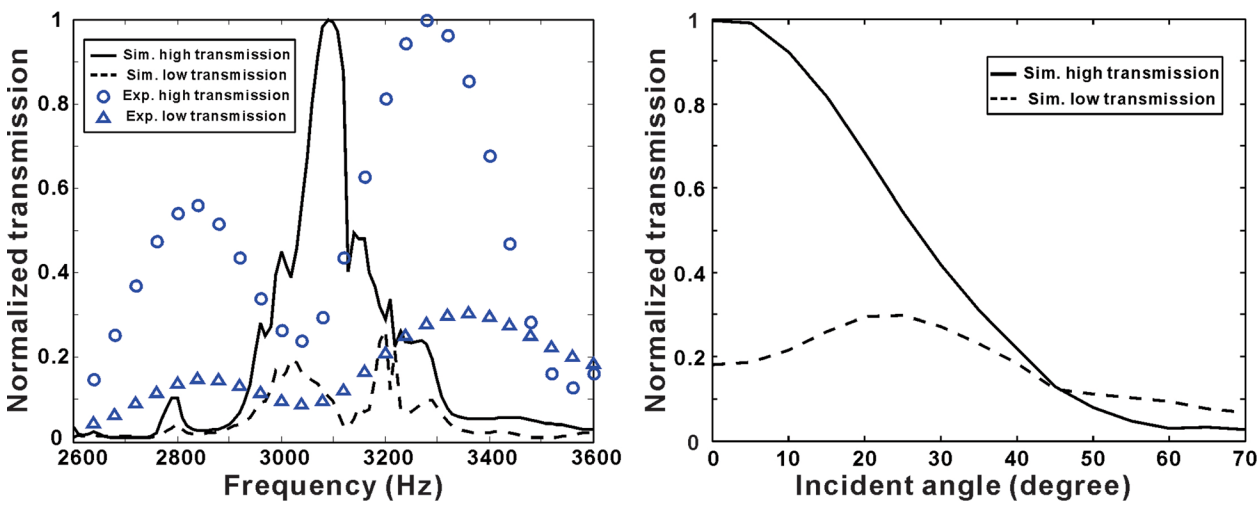

FIG. 6. (a). Normalized intensity transmission for different directions of incoming waves. (b) Normalized intensity transmission as a function of the incident angle.

Reuse of AIP Publishing content is subject to the terms at: https://publishing.aip.org/authors/rights-and-permissions. Download to IP: 152.14.115.167 On: Thu, 02 Jun 2016 18:24:35

fields at 3.28 kHz, which is the measured operating frequency as seen in Fig. 6(a). A reasonable agreement can be observed. The results indicate that the proposed device can yield an asymmetric transmission phenomenon for incident waves from different directions. The measured transmitted wavefront for the high transmission case is around 46°, which matches well with theory. Next, we integrated the total acoustic energy along a transverse line behind the sample. The overall normalized transmission is shown in Fig. 6(a) within the frequency band 2.6 kHz–3.6 kHz. The peak energy contrast is about four times in measurement, which is smaller than simulation (over ten times), and the optimal working frequency also has a certain shift from 3.1 kHz to 3.28 kHz. Several factors could contribute to these deviations between simulation and measurement. The peak energy contrast may be reduced in measurements because some leakage may have occurred inside the metasurfaces. This can also be caused by the imperfect boundary conditions of the 2D waveguide. The transmission may also be greater in simulation as it assumes no internal loss within the metasurfaces, which is inevitable in measurements.[29] The shift of operating frequency may be due to imperfection (e.g., fabrication errors of the space coiling geometry) and nonuniformity of the fabricated sample. To minimize the effect of loss in the proposed scheme, the labyrinthine structures may be replaced by low-loss membrane-type acoustic metamaterials.[26] It is also expected that more ZIM layers can be employed to yield a larger energy contrast, with the sacrifice of the device size. Numerical simulations are also performed to study the performance of the proposed device as a function of the incident angle. The normalized transmission is shown in Fig. 6(b) at 3.1 kHz. As expected, the transmission for the high transmission direction reaches its highest value at 0° and decreases quickly when the incident angle becomes larger. The device appears to have acceptable performance when the incident angle is less than around 10°.

It is worth pointing out that due to the dispersive nature of the ZIM structure, the near-zero refractive index occurs only within a relatively narrow frequency band, as illustrated in Fig. 3. The operating bandwidth of the proposed device is thus mainly limited by the performance of the ZIM. For the GIM, its performance can be preserved within a certain frequency band, which is wider than the ZIM.[20]

To conclude, we have designed, fabricated, and experimentally characterized dual-layer thin acoustic metasurfaces which exhibit asymmetric transmission within a certain frequency band. The effect is realized by total reflection for oblique incidence and tunneling for normal incidence induced by the ZIM. The device has a flat geometry and can be also readily modified to achieve asymmetric transmission for 3D wave propagation. It is hoped that this design can be helpful in noise control and architectural acoustics by rejecting the unwanted acoustic waves from selected directions. The design may also find applications in therapeutic ultrasound, acoustic sensors, and energy harvesting.[30] For example, the reflected wave in therapeutic ultrasound will be filtered out so that it will not interfere with the incident wave and generate standing waves, which may be harmful to tissue.

This work was partially supported by the Multidisciplinary University Research Initiative grant from the Office of Naval Research (N00014-13-1-0631).

[1]F. D. M. Haldane and S. Raghu, Phys. Rev. Lett. **100**, 013904 (2008).
[2]L. Feng, M. Ayache, J. Huang, Y.-L. Xu, M.-H. Lu, Y.-F. Chen, Y. Fainman, and A. Scherer, Science **333**, 729 (2011).
[3]B. Liang, B. Yuan, and J. C. Cheng, Phys. Rev. Lett. **103**, 104301 (2009).
[4]B. Liang, X. S. Guo, J. Tu, D. Zhang, and J. C. Cheng, Nat. Mater. **9**, 989 (2010).
[5]X. F. Li, X. Ni, L. Feng, M. H. Lu, C. He, and Y. F. Chen, Phys. Rev. Lett. **106**, 084301 (2011).
[6]Z. He, S. Peng, Y. Ye, Z. Dai, C. Qiu, M. Ke, and Z. Liu, Appl. Phys. Lett. **98**, 083505 (2011).
[7]R. Q. Li, B. Liang, Y. Li, W. W. Kan, X. Y. Zou, and J. C. Cheng, Appl. Phys. Lett. **101**, 263502 (2012).
[8]B. Yuan, B. Liang, J. C. Tao, X. Y. Zou, and J. C. Cheng, Appl. Phys. Lett. **101**, 043503 (2012).
[9]Y. Li, B. Liang, Z. M. Gu, X. Y. Zou, and J. C. Cheng, Appl. Phys. Lett. **103**, 053505 (2013).
[10]B.-I. Popa and S. A. Cummer, Nat. Commun. **5**, 3398 (2014).
[11]R. Fleury, D. L. Sounas, C. F. Sieck, and M. R. Haberman, Science **343**, 516 (2014).
[12]Y.-F. F. Zhu, X.-Y. Y. Zou, B. Liang, and J.-C. C. Cheng, Appl. Phys. Lett. **107**, 113501 (2015).
[13]Y. F. Zhu, X. Y. Zou, B. Liang, and J. C. Cheng, Appl. Phys. Lett. **106**, 173508 (2015).
[14]Z. Yang, F. Gao, X. Shi, X. Lin, Z. Gao, Y. Chong, and B. Zhang, Phys. Rev. Lett. **114**, 114301 (2015).
[15]A. B. Khanikaev, R. Fleury, S. H. Mousavi, and A. Alù, Nat. Commun. **6**, 8260 (2015).
[16]A. A. Maznev, A. G. Every, and O. B. Wright, Wave Motion **50**, 776 (2013).
[17]Y. Li, X. Jiang, R. Q. Li, B. Liang, X. Y. Zou, L. L. Yin, and J. C. Cheng, Phys. Rev. Appl. **2**, 064002 (2014).
[18]Y. Li, X. Jiang, B. Liang, J. Cheng, and L. Zhang, Phys. Rev. Appl. **4**, 024003 (2015).
[19]K. Tang, C. Qiu, M. Ke, J. Lu, Y. Ye, and Z. Liu, Sci. Rep. **4**, 6517 (2014).
[20]Y. Xie, W. Wang, H. Chen, A. Konneker, B.-I. Popa, and S. A. Cummer, Nat. Commun. **5**, 5553 (2014).
[21]Y. Cheng, C. Zhou, B. G. Yuan, D. J. Wu, Q. Wei, and X. J. Liu, Nat. Mater. **14**, 1013 (2015).
[22]N. Yu, P. Genevet, M. A. Kats, F. Aieta, J.-P. Tetienne, F. Capasso, and Z. Gaburro, Science **334**, 333 (2011).
[23]F. Liu, X. Huang, and C. T. Chan, Appl. Phys. Lett. **100**, 071911 (2012).
[24]Y. Jing, J. Xu, and N. X. Fang, Phys. Lett. A **376**, 2834 (2012).
[25]Z. Liang and J. Li, Phys. Rev. Lett. **108**, 114301 (2012).
[26]S. Zhai, H. Chen, C. Ding, F. Shen, C. Luo, and X. Zhao, Appl. Phys. A **120**, 1283 (2015).
[27]Y. Xie, B.-I. Popa, L. Zigoneanu, and S. A. Cummer, Phys. Rev. Lett. **110**, 175501 (2013).
[28]V. Fokin, M. Ambati, C. Sun, and X. Zhang, Phys. Rev. B **76**, 144302 (2007).
[29]G. P. Ward, R. K. Lovelock, A. R. J. Murray, A. P. Hibbins, J. R. Sambles, and J. D. Smith, Phys. Rev. Lett. **115**, 044302 (2015).
[30]R. Fleury, D. L. Sounas, M. R. Haberman, and A. Alù, Acoust. Today **11**, 14 (2015).

Reuse of AIP Publishing content is subject to the terms at: https://publishing.aip.org/authors/rights-and-permissions. Download to IP: 152.14.115.167 On: Thu, 02 Jun 2016 18:24:35